Presented at the 37th European PV Solar Energy Conference and Exhibition, 7-11 September 2020

ENABLING THE IN-SITU STRESS AND TEMPERATURE MEASUREMENT BY SILICON SOLAR CELL INTEGRATED STRESS AND TEMPERATURE SENSORS FOR PHOTOVOLTAIC MODULES

Andreas J. Beinert[1,2], Mark Imm[1,3], Jan Benick[1], Felix Becker[3], Sonja Seitz[1], Martin Heinrich[1], Oliver Paul[3], Stefan W. Glunz[1,4], Jarir Aktaa[2], Ulrich Eitner[1] and Holger Neuhaus[1]

[1] Fraunhofer Institute for Solar Energy Systems ISE, Heidenhofstrasse 2, 79110 Freiburg, Germany

[2] Karlsruhe Institute of Technology (KIT), Institute for Applied Materials, Hermann-von-Helmholtz-Platz 1, 76344 Eggenstein-Leopoldshafen, Germany

[3] University of Freiburg, Department of Microsystems Engineering (IMTEK), Georges-Koehler-Allee 103, 79110 Freiburg, Germany

[4] University of Freiburg, Department of Sustainable Systems Engineering (INATECH), Emmy-Noether-Strasse 2, 79110 Freiburg, Germany

Corresponding author: Andreas J. Beinert | Phone: +49 (0)761 4588 5630 | E-mail: Andreas.Beinert@ise.fraunhofer.de

ABSTRACT: We propose silicon solar cell integrated stress and temperature sensors as a new approach for the stress and temperature measurement in PV modules. The solar cell integrated sensors enable a direct and continuous in-situ measurement of mechanical stress and temperature of solar cells within PV modules. In this work, we present a proof of concept for stress and temperature sensors on a silicon solar cell wafer. Both sensors were tested in a conventional PV module setup. For the stress sensor, a sensitivity of (-47.41 ± 0.14) %/GPa and for the temperature sensor a sensitivity of (3.557 ± 0.008) × $10^{-3}K^{-1}$ has been reached. These sensors can already be used in research for increased measurement accuracy of the temperature and the mechanical stress in PV modules due to the implementation at the precise location of the solar cells within a laminate stack, for process evaluation, in-situ measurements in reliability tests and the correlation with real exposure to climates.

Keywords: stress measurement, temperature measurement, stress sensor, temperature sensor, PV module, in-situ measurement, predictive maintenance

1 INTRODUCTION

Degradation of photovoltaic (PV) modules in the field still leads to a significant power loss of PV systems [1–4]. Moreover, the detection of degradation is often related to elaborate and time-consuming characterization methods. Amongst them are visual inspection, IV curve analysis, electroluminescence imaging, thermography and UV fluorescence [2]. However, they all detect the degradation effect, not the stress origin. There are also a few methods known for a predictive failure analysis, e.g. using thermography in combination with smart algorithms [5] or maximum power point tracking (MPPT) [6]. However, the thermography is not capable for a continuous analysis and the MPPT only detects failures when they occur.

We propose a different and novel approach for in-situ monitoring and predictive maintenance analysis: sensors which are integrated into the solar cell itself. The advantage of solar cell integrated sensors is the possibility of continuous in-situ measurements on cell level. In this work, we present first results of stress and temperature sensors, which are integrated into silicon solar cell wafers and hence measure the stress and temperature of the solar cell wafer itself. The presented sensors have the purpose to be used in research and development, for example in mechanical load or thermal cycling tests according to IEC 61215 [7]. They can help to obtain a deeper understanding of the module technology and investigate the influence of new solar cell or module concepts on it. Possible applications are the development of lightweight PV modules or the heating of solar cells by reverse operation. Further research will focus on transferring the sensors to functional solar cells and a use in conventional PV modules.

Each sensor covers only a small part of the solar cell, hence the interaction with the solar cell and the PV module is minimized, which is the requirement for a reasonable in-situ measurement. Both sensors can be manufactured by using processes typically applied in the solar cell production. Hence, they can be applied to all silicon based solar cells, either on the front or back side. Also existing solar cell production lines could be modified for the sensor implementation.

This is a condensed version of a published open access article, therefore we refer to [8] for the full details.

2 STRESS SENSOR

Cell cracks induced by tensile stress [9,10], can account for PV module degradation rates of up to 8% relative power loss per year [1]. Recently (synchrotron) X-ray [11,12] and Raman microdiffraction [13–17] were presented as methods to measure the stress in solar cells encapsulated in a PV module. Both methods are capable of measuring the residual stress in solar cells. However, since they are based on the interaction of light with solar cells, the measurement has to be performed with a special setup and usually in a laboratory. Consequently, in-situ measurements are very challenging for these methods. Another optical method used previously is the measurement of the cell gap displacement by digital image correlation [18]. Since this is also an optical method the same restrictions apply. A non-optical method would be the use of foil strain gauges, which have several disadvantages. For example, the foil strain gauge is adhered to the encapsulant and the solar cell, therefore the strain in the gauge cannot be assigned to one layer. In addition, inserting the foil strain gauge into the laminate modifies its thermomechanical properties.

To overcome these issues, we have developed a piezoresistive stress sensor, which is integrated into the

silicon solar cell wafer. Therefore, it measures the stress in the solar cell itself without interfering with it. The sensor is based on the piezoresistance effect of silicon which is well-known and used for sensor applications in the field of microelectronics [19–22]. We transfer the method to p-type monocrystalline silicon solar cell wafers and use lab-scale silicon solar cell production technologies. The stress sensor is realized as a rectangular piezoresistive resistor using high local n-doping by ion-implantation, as depicted in Figure 1. The same process is used to generate local passivated contacts in silicon solar cells and subsequent silver metallization. To shield the sensor from the electrons generated in the adjacent silicon, a highly p-doped shielding guard-ring (set to ground in the characterization measurements) is implemented around the sensor.

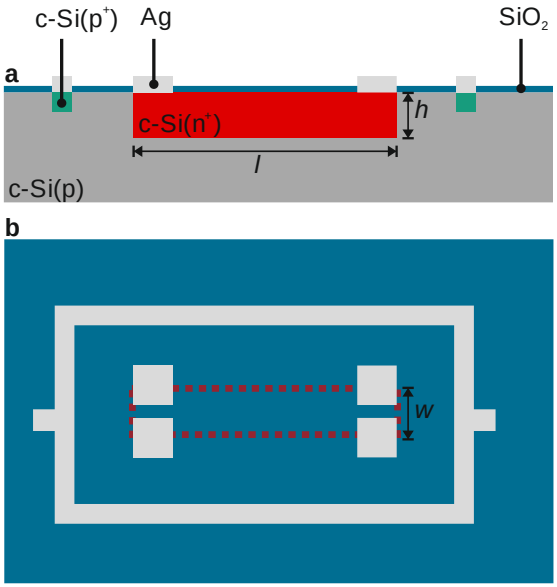

Figure 1: Schematic drawing of the piezoresistive stress sensor. **a**: Cross-sectional view, the sensor consists of a highly n-doped area within the p-doped substrate and a highly p-doped shielding ring. Both are contacted by Ag metallization. **b**: Top view: the p-doped area of the shielding is hidden by the metallization. The dotted line indicates the shape of the piezoresistive sensor part, which is hidden by the SiO2 layer, not to scale. [8]

2.1 Method

For a uniaxial stress σ_{xx} the change in resistance ΔR_σ of a rectangular piezoresistor depends on the sheet resistance $R_\square$ of the n-doped layer, its length l and width w, the piezoresistive coefficient at room temperature $\pi_{11,\mathrm{ref}}$ and the dimensionless factor P, which describes the dependency of temperature T and the charge carrier concentration N:

$$\Delta R_\sigma = R_\square \frac{l}{w} \pi_{11,\mathrm{ref}} P(T,N)\, \sigma_{xx}. \qquad (1)$$

For sufficiently high charge carrier concentrations ($\gg 10^{20}$ cm^{-3}) the temperature dependence vanishes [23].

We use a target sheet resistance $R_\square$ of 100 Ω/sq and vary the aspect ratio $a = l/w$ as well as the charge carrier concentration N. Table I shows the chosen design variations.

The sensors were produced at the Fraunhofer Institute for Solar Energy Systems ISE on p-type float zone silicon solar wafers with a specific resistance of 1 Ωcm and a thickness of 250 µm. On each wafer, 40 sensors were placed in a way that the wafer can be cut into stripes containing four sensors.

Table I: Design variations of the stress sensor.

Variation	Charge carrier concentration N [cm^{-3}]	Aspect ratio a [-]	Resistance R_σ [Ω]
S.1	1×10^{19}	5	500
S.2	1×10^{19}	10	1000
S.3	1×10^{19}	50	5000
S.4	5×10^{19}	5	500
S.5	5×10^{19}	10	1000
S.6	5×10^{19}	50	5000

For the characterization on a four-point bending bridge [24], we split the wafers into single stripes of 10×100 mm^2 using a laser. The current-voltage characteristics was measured for two sensors at a time. The distance of the four-point bending supports were set so that both sensors are exposed to the same stress. In pretests, we found that the sensor stripes fracture at around 90 MPa; therefore we limit the test range to 65 MPa and subdivide it into 13 load steps. At each load step the current at an applied voltage of 1 V is measured by an electrical four-point probe. From the data, we calculate the change of resistance ΔR_σ relative to 0 MPa. We then plot the relative resistance change $\Delta R_\sigma / R_{\sigma,0}$ over the uniaxial stress σ_{xx} (see Figure 2). Finally, we evaluate the sensitivity S_σ of the sensor by performing a linear fit with:

$$S_\sigma = \frac{\Delta R_\sigma}{R_{\sigma,0}\, \Delta\sigma_{xx}}. \qquad (2)$$

We have characterized between 10 and 19 sensors of each design variation.

2.2 Results and discussion

Figure 2 exemplarily shows the relative resistance change of one sensor type from variation S.5. As predicted by equation (1), the resistance shows a linear dependency on the applied stress.

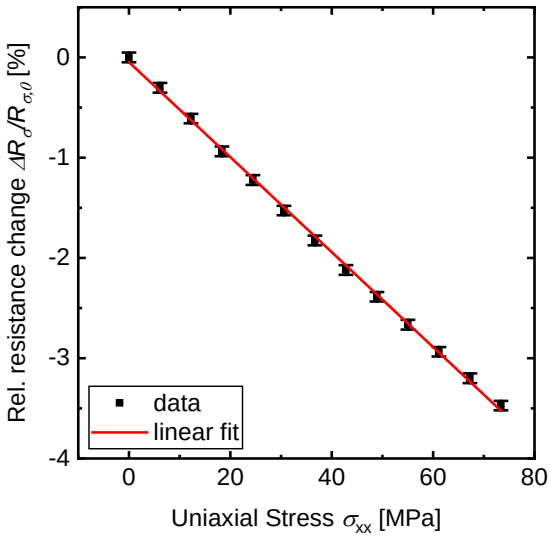

Figure 2: Relative resistance change vs. uniaxial stress for one exemplary sensor from variation S.5. The solid red line is a linear fit to the data from which the sensitivity S_σ is obtained. [8]

Design variation S.5 (a = 10/1, N = 5×10^{19} cm^{-3}) has the smallest deviation, therefore we choose to further investigate this design. It has a sensitivity of (-47.41 ± 0.14) %/GPa.

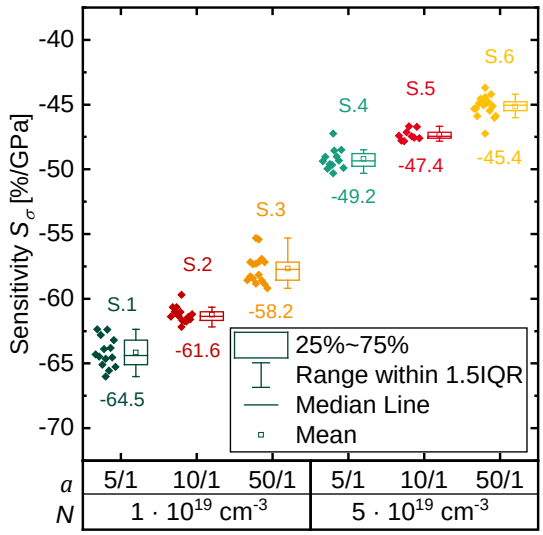

Figure 3: Sensitivity of the six different stress sensor variations. On the x-axis are the aspect ratio a and the charge carrier concentration N. The box is the interquartile range (IQR), i.e. the range in which the middle 50% of the data lie, the line within the box is the median and the square is the mean, the whiskers show the range in which 1.5·IQR of the data lie. [8]

Module integration

We laminate the chosen sensor design S.5 using a conventional PV module setup (Figure 4), with a 14.7x10.5 cm^2 and 1 mm thin glass, EVA and a TPT backsheet.

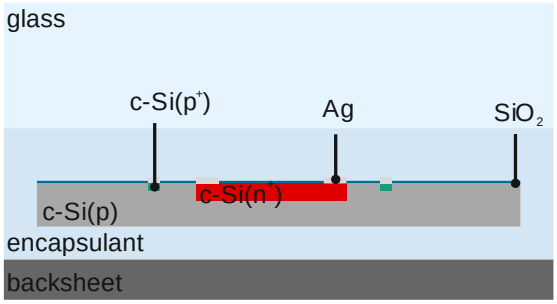

Figure 4: Setup of the laminated sensor stripe. A standard glass-foil setup is used with EVA as encapsulant and a 1 mm thin glass, not to scale. [8]

The resistance change ΔR_σ during a three-point bending test to failure is measured and interconverted to stress using above sensitivity. We have obtained a linear correlation between the deflection and the relative change in resistance. The interconversion into stress reveals that the silicon stripe is in compressive stress, which is shown in Figure 5. The step at around 0.6 mm deflection originates from a small fracture of the glass, the solder joint, metallization or the silicon stripe, which does not affect the sensors performance, but induces a sudden change of the measured resistance and hence the calculated stress. However, the stress value change is only 0.5 MPa and therefore is insignificant. The successful measurement of bending stress proves that the proposed sensor is capable to determine stress within a PV module setup.

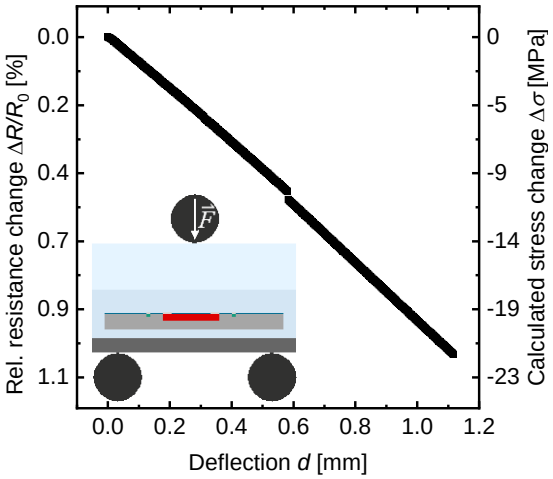

Figure 5: Stress measured in a laminated sensor stripe in three-point bending. The stress change is calculated from the relative resistance change $\Delta R_\sigma/R_{\sigma,0}$ using a sensitivity S_σ of -47.41 %/GPa. The insert shows the three-point bending setup schematically; please note that the left axis is reversed. [8]

3 TEMPERATURE SENSOR

The PV modules temperature influences not only the reliability but also its performance [25]. Accordingly, several methods were proposed to determine the PV module temperature in the past. The most common method is the use of temperature sensors such as thermocouples [25–27], which are either laminated into or attached to the rear side of the PV module. The former has the disadvantage that the PV module setup is modified by the sensor and due to its height, the temperature cannot be assigned to one layer. The latter does not allow an accurate temperature measurement within the PV module [27]. Another approach is infrared (IR) imaging [26], which is capable of resolving the temperature of solar cells. However, IR imaging for permanent measurements during operation and testing is rather costly and therefore applied occasionally, only. Also the silicon solar cell itself is used as a temperature sensing device by utilizing the temperature dependency of the voltage [26]. However, since the voltage depends on various factors, the operation conditions, especially the irradiation, need to be determined as well.

We present a temperature sensor, which can be integrated on the silicon solar cell itself. Hence, it can measure the solar cell temperature directly without interfering with the PV module setup. Figure 6 shows a schematic drawing of the proposed design.

3.1 Method

We utilize the temperature sensitivity of the silver used for metallization and develop a sensor equivalent to a Pt100 sensor. Accordingly we design a structure with a nominal resistance $R_{T,0}$ at 0 °C of 100 Ω. The resistance $R_{T,0}$ depends on the specific resistance ρ, length l, width w and height h:

$$R_{T,0} = \rho \frac{l}{h\,w}. \qquad (3)$$

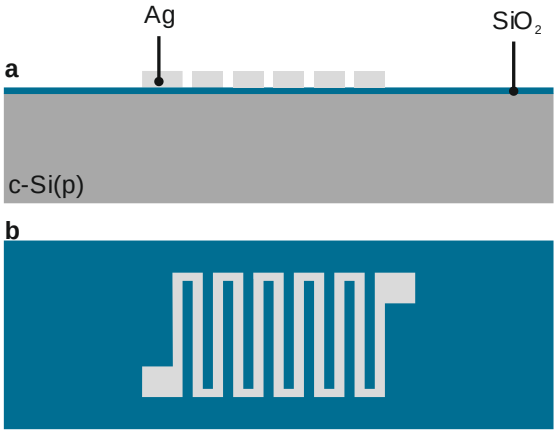

Figure 6: Schematic drawing of the resistive temperature sensor. **a:** Cross-sectional view with the metallization insulated from the substrate by silicon oxide. **b:** Top view with the meander like structure of the metallization, not to scale. [8]

The temperature dependence is expressed by the resistance temperature coefficient α_T:

$$R_T(T) = R_{T,0}(1 + \alpha_T\, T), \qquad (4)$$

where $R_{T,0}$ and α_T are defined for 0 °C, and T denotes temperature in °C.

Due to the relatively low specific resistance ρ of silver of about 1.6×10^{-5} Ωmm [28], the sensor is designed as a meander to allow a small size while achieving a resistance of 100 Ω. The silicon oxide layer is used as an electrical insulation layer from the sensor cell.

The sensors are manufactured on the same solar cell wafer as the stress sensors at Fraunhofer ISE. We use the same process as for the stress sensor metallization. This technique is commonly used for contact formation of high-efficiency solar cells.

Characterization

We measure the resistance R_T using an electrical four-point probe setup during three temperature cycles in the range of -40…+160 °C for eight different sensors. The actual temperature is measured with at least two type K thermocouples. In each cycle, we increase the temperature in steps of 10 K with a slope of 2 K/min and hold it for 10 min before the measurement to have a stable temperature during the measurement. We then plot the measured resistance R_T versus the temperature (see Figure 8) and finally determine the sensitivity S_T, which is the resistance temperature coefficient α_T, by a linear fit:

$$S_T = \alpha_T = \frac{\Delta R_T}{R_{T,0}\,\Delta T}. \qquad (5)$$

We determine the resistance temperature coefficient α_T for each cycle for the heating and cooling phase separately. For each sensor, we draw the mean over all cycles and phases and finally over all eight sensors.

Module integration

We laminate one silicon stripe containing three temperature sensors using above mentioned standard PV module setup (Figure 4) with a 20×20 cm^2 front glass of 3 mm thickness. Next to the sensor stripe, we place two type K thermocouples. We then expose the laminated sensor stripe to 145 accelerated temperature cycles (aTC) [29] between -35 °C and +85 °C with a slope of 8.3 K/min and a holding time at the minimum and maximum temperature of 15 min. Using an electrical four-point probe, we measure the resistance each 1.5 min.

3.2 Results and discussion

Characterization

The variance of the eight sensors is not significant. Therefore, exemplarily results of Sensor 1 are shown in Figure 8. The mean resistance temperature coefficient α_T is $(3.557 \pm 0.008)\ 10^{-3}\mathrm{K}^{-1}$. The mean value of $R_{T,0}$ is (100.6 ± 0.3) Ω.

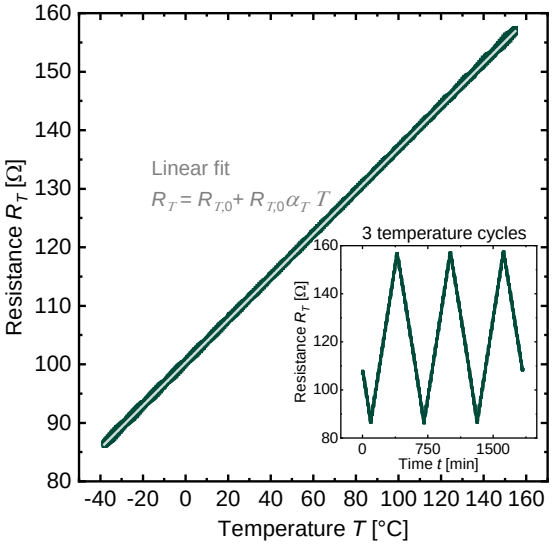

Figure 7: Temperature dependent resistance R_T of one exemplary temperature sensor. The data represents three temperature cycles shown in the insert. The line is a linear fit. [8]

Module integration

Figure 9 shows the relative change of the 0 °C resistance $R_{T,0}$ and of the temperature coefficient α_t each 10$^{\text{th}}$ cycle.

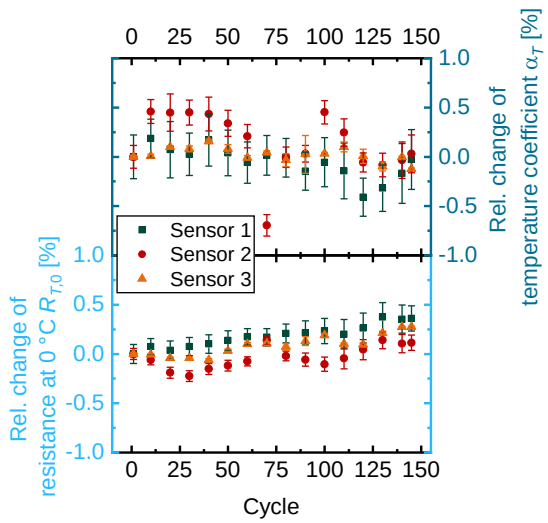

Figure 8: Change of 0 °C resistance $R_{T,0}$ (bottom) and the resistance temperature coefficient α_T (top) for three module integrated sensors during 145 thermal cycles. The values are evaluated each 10 cycles, the change is relative to the first cycle. [8]

The results indicate a slight increase of less than 0.5% of the 0 °C resistance $R_{T,0}$, most likely due to a slight degradation of the solder joint. However, the temperature coefficient α_T does not show this systematic change. We chose a fairly high temperature gradient during the thermal cycles to minimize the testing time. Consequently, the variability of the temperature coefficient α_t is up to 0.75%. Since this is still a relatively low value and the temperature gradient occurring in the field are lower, we conclude, that the sensors are capable to determine the temperature of silicon solar cells within a PV module.

4 CONCLUSION

We propose a new approach for in-situ and predictive maintenance measurements of PV modules: silicon solar cell integrated sensors. In this work, we present a stress and a temperature sensor, which are integrated in silicon solar cell wafers. The sensors are manufactured using only silicon solar cell production processes.

The stress sensor utilizes the piezoresistance effect of silicon at high local doping. The presented sensors are produced on p-doped float zone solar cell wafers. Accordingly, the sensing part consists of a highly n-doped area. Six different designs with varying aspect ratio a and charge carrier concentration N are compared. All designs resolve the stress in the test specimens and have sensitivities in the range between -45 and -65 %/GPa. The lowest scattering is achieved for the design with a = 10/1, $N = 5 \times 10^{19}$ cm^{-3}, which has a sensitivity of (-47.41 ± 0.14) %/GPa. The module integration of this design shows that the sensors are capable of measuring the stress in laminated solar cells.

The temperature sensor utilizes the temperature dependence of the silver metallization. We propose a meander style design with a 0 °C resistance of 100 Ω. The produced sensors have a value of (100.6 ± 0.3) Ω with a resistance temperature coefficient α_T, which is the sensitivity of the sensors, of $(3.557 \pm 0.008)\ 10^{-3}\text{K}^{-1}$. Laminated sensors show a good stability in 145 temperature cycles from -35 °C to +85 °C. Therefore, we conclude that the proposed sensors are indeed capable of measuring the temperature in laminated silicon solar cells.

The presented sensors can already be applied in research and development for in-situ monitoring in accelerated testing, such as monitoring temperature and stress in laminates precisely at the location of solar cells. In further works, we implement the sensors on electrically functional solar cells. These sensors integrated in solar cells (SenSoCell®) will enable an integrated direct and continuous in-situ monitoring of the solar cells stress and temperature within a PV module. Further research is ongoing on solar cell integrated moisture sensors, which enable a direct measurement of the moisture content of the encapsulant.

5 ACKNOWLEDGEMENT

This work was supported by a PhD scholarship from the Cusanuswerk in Bonn, Germany.

6 REFERENCES

[1] M. Köntges, G. Oreski, U. Jahn, M. Herz, P. Hacke, Weiss Karl-Anders, G. Razongles, M. Paggi, D. Parlevliet, T. Tanahashi, French, Roger, H. Assessment of Photovoltaic Module Failures in the Field. Report IEA-PVPS T13-09:2017 (2017).

[2] M. Köntges, S. Altmann, T. Heimberg, U. Jahn, K.A. Berger, Proceedings of the 32nd European Photovoltaic Solar Energy Conference and Exhibition (EU PVSEC) (2016), 1435–1443.

[3] D.C. Jordan, S.R. Kurtz, K. VanSant, J. Newmiller, Prog. Photovolt: Res. Appl. 24 (2016), 978–989.

[4] D.C. Jordan, S.R. Kurtz, Prog. Photovolt: Res. Appl. 21 (2013), 12–29.

[5] Z.A. Jaffery, A.K. Dubey, I. Kahn, A. Haque, Infrared Phys. Technol. 83 (2017), 182–187.

[6] E. Roman, R. Alonso, P. Ibanez, S. Elorduizapatarietxe, D. Goitia, IEEE Trans. Ind. Electron. 53 (2006), 1066–1073.

[7] IEC IEC 61215-2:2016, Terrestrial photovoltaic (PV) modules – Design qualification and type approval – Part 2: Test procedures (2016).

[8] A.J. Beinert, M. Imm, J. Benick, F. Becker, S. Seitz, M. Heinrich, O. Paul, S.W. Glunz, J. Aktaa, U. Eitner, H. Neuhaus, Prog. Photovolt: Res. Appl. 28 (2020), 717–724.

[9] M. Köntges, I. Kunze, S. Kajari-Schroeder, X. Breitenmoser, B. Bjørneklett, Sol Energ Mat Sol C 95 (2011), 1131–1137.

[10] F. Kaule, W. Wang, S. Schönfelder, Sol Energ Mat Sol C 120, Part A (2014), 441–447.

[11] V.A. Handara, I. Radchenko, S.K. Tippabhotla, K. R.Narayanan, G. Illya, M. Kunz, N. Tamura, A.S. Budiman, Sol Energ Mat Sol C 162 (2017), 30–40.

[12] X. Meng, M. Stuckelberger, L. Ding, B. West, A. Jeffries, M. Bertoni, IEEE J. Photovolt. 8 (2018), 189–195.

[13] W. Mühleisen, J. Schicker, L. Neumaier, C. Hirschl, N. Vollert, S. Seufzer, R. Battistutti, M. Pedevilla, J. Scheurer, M. Schwark, T. Fischer, Proceedings of the 31st European Photovoltaic Solar Energy Conference and Exhibition (EU PVSEC) (2015), 160–163.

[14] A. Büchler, A.J. Beinert, S. Kluska, V. Haueisen, P. Romer, F.D. Heinz, M. Glatthaar, M.C. Schubert, Enrgy Proced 124 (2017), 18–23.

[15] A.J. Beinert, P. Romer, A. Büchler, V. Haueisen, J. Aktaa, U. Eitner, Enrgy Proced 124 (2017), 464–469.

[16] A.J. Beinert, A. Büchler, P. Romer, M. Heinrich, M.C. Schubert, J. Aktaa, U. Eitner, Proceedings of the 7th World Conference on Photovoltaic Energy Conversion (WCPEC-7) (2018), 3613–3617.

[17] A.J. Beinert, A. Büchler, P. Romer, V. Haueisen, L.C. Rendler, M.C. Schubert, M. Heinrich, J. Aktaa, U. Eitner, Sol Energ Mat Sol C 193 (2019), 351–360.

[18] U. Eitner, M. Köntges, R. Brendel, Sol Energ Mat Sol C 94 (2010), 1346–1351.

[19] P. Gieschke, O. Paul, Procedia Engineering 5 (2010), 1364–1367.

[20] P. Gieschke, B. Sbierski, O. Paul, Proceedings of the IEEE Sensors 2011 (2011), 93–96.

[21] J.C. Suhling, R.C. Jaeger, IEEE SENS J 1 (2001), 14–30.

[22] J.L. Spencer, W.F. Schroen, G.A. Bednarz, J.A.

Bryan, T.D. Metzgar, R.D. Cleveland, D.R. Edwards, Proceedings of the 19th International Reliability Physics Symposium (1981), 74–80.
[23] Y. Kanda, Sensors and Actuators A 28 (1991), 83–91.
[24] F. Becker, M. Kuhl, Y. Manoli, O. Paul, Proceedings of the IEEE Sensors 2015 (2015), 1–4.
[25] D.L. King, J.A. Kratochvil, W.E. Boyson, Conference record of the twenty sixth IEEE Photovoltaic Specialists Conference - 1997: Anaheim Marriott, Anaheim, CA, 29 September-03 October 1997 (1997), 1183–1186.
[26] J.D. C. R., K. M, B. George, J. Kumar V, IEEE International Instrumentation and Measurement Technology Conference (I2MTC), 2012 (2012), 1847–1850.
[27] N. Umachandran, G. TamizhMani, Proceedings of the 43rd IEEE Photovoltaic Specialists Conference (IEEE PVSC) (2016), 2731–2737.
[28] J.R. Rumble CRC handbook of chemistry and physics, 98th ed., CRC Press, Boca Raton, Florida (2017).
[29] C.H. Schiller, L.C. Rendler, D. Eberlein, G. Mülhöfer, A. Kraft, D.H. Neuhaus, Proceedings of the 36th European Photovoltaic Solar Energy Conference and Exhibition (EU PVSEC) (2019), 995–999.